JBC RESEARCH ARTICLE

Mutational widening of constrictions in a formate–nitrite/H^+ transporter enables aquaporin-like water permeability and proton conductance

Received for publication, October 4, 2021, and in revised form, December 14, 2021 Published, Papers in Press, December 18, 2021,
https://doi.org/10.1016/j.jbc.2021.101513

Jana D. R. Schmidt and Eric Beitz*

From the Department of Pharmaceutical and Medicinal Chemistry, Christian-Albrechts-University of Kiel, Kiel, Germany

Edited by Karen Fleming

The unrelated protein families of the microbial formate–nitrite transporters (FNTs) and aquaporins (AQP) likely adapted the same protein fold through convergent evolution. FNTs facilitate weak acid anion/H^+ cotransport, whereas AQP water channels strictly exclude charged substrates including protons. The FNT channel–like transduction pathway bears two lipophilic constriction sites that sandwich a highly conserved histidine residue. Because of lacking experiments, the function of these constrictions is unclear, and the protonation status of the central histidine during substrate transport remains a matter of debate. Here, we introduced constriction-widening mutations into the prototypical FNT from *Escherichia coli*, FocA, and assayed formate/H^+ transport properties, water/solute permeability, and proton conductance. We found that enlargement of these constrictions concomitantly decreased formate/formic acid transport. In contrast to wild-type FocA, the mutants were unable to make use of a transmembrane proton gradient as a driving force. A construct in which both constrictions were eliminated exhibited water permeability, similar to AQPs, although accompanied by a proton conductance. Our data indicate that the lipophilic constrictions mainly act as barriers to isolate the central histidine from the aqueous bulk preventing protonation *via* proton wires. These results are supportive of an FNT transport model in which the central histidine is uncharged, and weak acid substrate anion protonation occurs in the vestibule regions of the transporter before passing the constrictions.

Formate–nitrite transporters (FNTs) bidirectionally translocate small weak monoacids, such as formic/acetic/lactic/nitric/hydrosulfuric acid across microbial cell membranes (1). The bacterial FocA isoform for instance plays key roles in the production of hydrogen from formic acid (2) and in the release of metabolites derived from mixed acid fermentation (3). Bacterial nitric acid–transporting FNTs (NirC) are part of the global nitrogen cycle (4). FNT-facilitated export of lactic acid is vital for protozoan malaria parasites of the genus *Plasmodium* rendering them valid novel drug targets (5–8). Curiously, despite unrelated functions and protein sequences, the FNTs have adapted the same general protein fold (9) as the aquaporin (AQP) channels for water and neutral solutes (10).

FNT and AQP protomers alike span the lipid bilayer six times (Fig. 1*A*). The transmembrane helices are tilted in a right-handed manner around a central substrate transduction pathway. A peculiar structural element shared by both protein families is a seventh pseudotransmembrane helix that is formed by two short so-called half-helices whose positive ends meet halfway in the membrane (9, 10). FNTs assemble into homopentamers and AQPs into homotetramers with each protomer acting as an individual substrate translocation unit rather than the central pore of the complex (9, 10).

Despite an overall identical fold, the inner workings of the FNTs and AQPs are distinct because of specific structure features that enable attraction, selection, and passage of the different types of substrates (11). The FNT transduction pathway is symmetrical with respect to the extracellular and cytosolic entrance sites (Fig. 1*A*). At both ends, positively charged lysine residues attract weak acid anions into funnel-like vestibules (11). A constriction site is formed on either side by bulky hydrophobic amino acid side chains (Fig. 1*B*) leaving open diameters smaller than the substrate in the *Escherichia coli* FocA crystal (Protein Data Bank [PDB] ID: 3KCU) (9). In order for a formate substrate molecule to pass the constrictions, the amino acid side chains move sideways in a flickering motion (12). The constriction sites sandwich a highly conserved histidine residue in the center of the transport path that is found in more than 98% of the FNTs (1) (Fig. 1*A*). Attempts to replace the histidine by other amino acids led to nonfunctional FNT proteins (11, 13, 14). There are, however, few natural FNT isoforms that are functional despite carrying a nonprotonatable central residue, for example, an asparagine (15).

The role of the central histidine and in particular its protonation status in the context of the FNT weak acid anion/H^+ cotransport mechanism is still a matter of debate. We favor a model, that is, the dielectric slide mechanism, in which the central histidine is uncharged (11, 16): A substrate anion enters one of the vestibules by electrostatic attraction where it encounters an increasingly lipophilic environment that decreases the acid strength of the substrate leading to protonation and formation of the neutral acid. The uncharged

* For correspondence: Eric Beitz, ebeitz@pharmazie.uni-kiel.de.

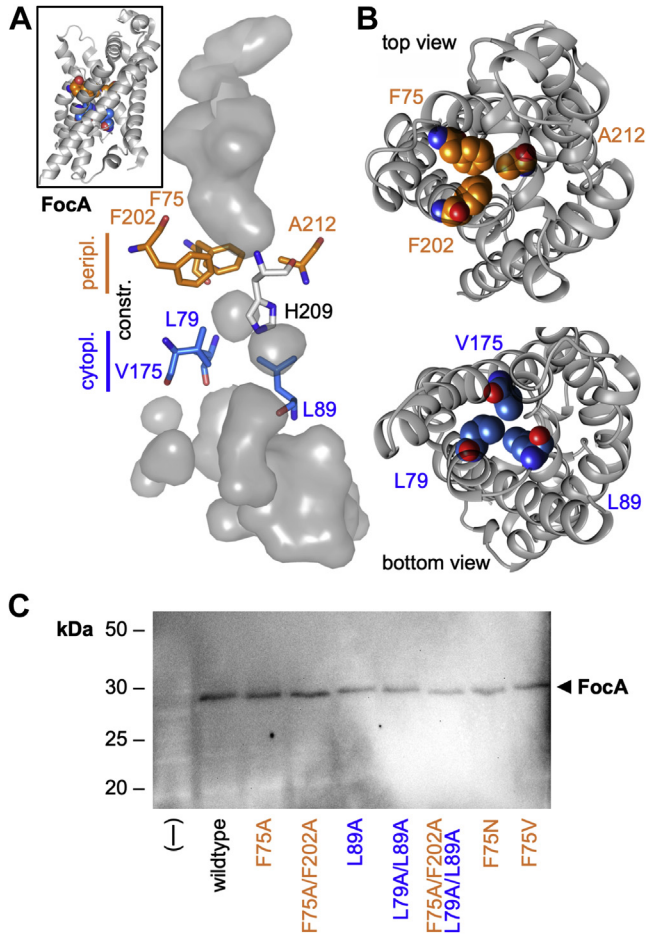

Figure 1. Structure of the FocA transport path. *A*, shown is the internal volume of the transport path of an FocA protomer (the *inset* shows a cartoon of the protomer; Protein Data Bank ID: 3KCU, chain A). The path is narrowed by bulky hydrophobic amino acid residues forming narrow constrictions toward the periplasmic (*orange*) and the cytoplasmic end (*blue*). A highly conserved histidine is located in the central region. *B*, the space-fill display of the constriction residues visualizes that widening side-chain movement is required to allow for substrate passage. *C*, Western blot showing yeast expression of FocA constriction site mutants probed with an antibody directed against N-terminally engineered hemagglutinin epitope tags. FocA, FNT-type formate transporter from *Escherichia coli*.

substrate can then pass the lipophilic constriction sites and the neutral central histidine region and will eventually dissociate into the anion and proton after leaving the transporter. Alternative models propose the central histidine to act as a proton acceptor and donor site independently from an entering substrate molecule (17). There are issues with this view concerning the question how a proton can travel across the lipophilic barriers, and whether the calculated high binding energy between a substrate anion and the protonated histidine would prevent further transport (18, 19).

In this study, we widened the constriction sites of the prototypical *E. coli* FocA by mutation and assayed formate/H^+ transport at different pH conditions. In addition, we tested the wildtype and mutant FocA variants for AQP-like channel properties. We found that opening up one of the constriction sites resulted in decreased pH-independent formate or formic acid transport. Eliminating both constrictions resulted in a loss of transport, yet concurrently, permeability for water and the neutral solute methylamine was initiated. Importantly, the new water permeability was accompanied by a proton leak through the protein. From this set of experiments, we conclude that a neutral central histidine is required for weak acid/H^+ transport by FNTs. The lipophilic FNT constriction sites block protons from entering the central histidine region by breaking water chains that would act as proton wires.

Results

Widening of the FocA constriction sites inhibits formate/formic acid transport

Initially, we generated mutants of *E. coli* FocA that carry a single replacement or a double replacement by alanine of the largest lipophilic residues at the periplasmic (F75, F202) or cytoplasmic constriction site (L79, L89). A quadruple mutant in which all four residues were changed to alanine was made in addition. We expressed wildtype and mutant FocA in *Saccharomyces cerevisiae* yeast (W303IA Δjen1 Δady2) that is devoid of endogenous monocarboxylate transporters (5). All constructs were evenly produced by the yeast strain as shown by Western blot (Fig. 1*C*). Similar mutations in earlier work affecting internal protein sites yet leaving the surface and termini unchanged were properly inserted into the plasma membrane as shown by microscopy and functional transport assays (5, 20). We tested for transport functionality of the mutants of this study by subjecting the yeast cells to a 1 mM inward gradient of ^{14}C-labeled formate at an external buffer pH of 6.8 using an established protocol for monocarboxylate transporters from bacteria, protozoa, and mammalia (5, 11, 20). Because of the absence of endogenous monocarboxylate transporters, the used yeast system produces minimal background. The formate concentration was chosen to match earlier studies using FocA and was expected to lie within the physiological range. Introduction of a single alanine, FocA F75A and FocA L89A, had little effect on the formate/formic acid transport functionality under these conditions (Fig. 2, *A*–*C*). In case of FocA F75A, the transport capacity even appeared increased (Fig. 2*B*). A similar behavior was reported before using related valine and alanine substitutions of FNT constriction site residues (9, 21). The authors explained the observed increase in transport capacity by less hindrance of a passing substrate molecule at the enlarged constrictions. However, and quite counterintuitively, we found that replacing two lipophilic residues of the same constriction site by alanine, FocA F75A/F202A and FocA L79A/L89A, greatly decreased transport (Fig. 2, *B* and *C*). In the latter case, transport was almost indiscernible from the background level. The quadruple alanine mutant FocA F75A/F202A–L79A/L89A appeared nonfunctional with respect to formate/formic acid transport (Fig. 2*D*).

FocA variants with widened constriction sites lose proton gradient–driven transport behavior

Previous electrophysiology measurements showed that FNTs leak substrate anions in the neutral pH range (12). When the cells are subjected to a transmembrane pH gradient, the

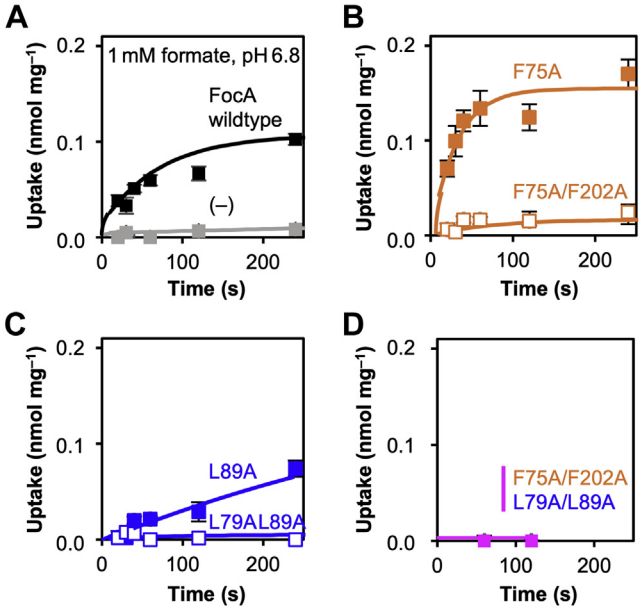

Figure 2. Formate/formic acid transport functionality. *A*, FocA wildtype mutants. *B–D*, constriction site mutants. Shown are uptake curves of ^{14}C-labeled formate into yeast cells (W303IA Δjen1 Δady2) expressing FocA or one of the variants (1 mM inward substrate gradient, buffer pH 6.8). The minimal background transport by the yeast strain devoid of endogenous monocarboxylate transporters (*A*, *gray curve*) was subtracted from the remaining curves. Error bars indicate SEM from three individual experiments each with triplicate data points. FocA, FNT-type formate transporter from *Escherichia coli*.

translocation mechanism changes to substrate anion/H^+ cotransport that is driven by the proton motive force (5, 11). We therefore assessed whether a widened constriction site affects the pH dependence of formate/formic acid transport. We used FocA constructs with mutations in the periplasmic constriction (F75A and F75A/F202A) and generated two more mutants to achieve intermediate diameters (F75N and F75V). The F75N asparagine replacement was chosen because it occurs naturally in the FNT from *Entamoeba histolytica* (15). Predictions of the resulting apertures are shown in Figure 3*A*. Analysis of FocA crystal data (PDB ID: 3KCU) (9) yielded a minimal open area in the periplasmic constriction region of 1.2 Å^2. Modeling of the constriction mutations indicated a stepwise increase of the areas to 15.9 Å^2 (F75N), 17.7 Å^2 (F75V), 23.6 Å^2 (F75A), and 42.3 Å^2 (F75A/F202A). We then determined the formate/formic acid uptake rates of wildtype and mutant FocA in the pH range of 4.8 to 7.3 (Fig. 3*B*). Wildtype FocA and the F75N mutant showed an equal rise in the uptake rates toward acidic conditions (Fig. 3*B*). FocA F75V and FocA F75A, however, were largely pH independent as seen by uptake rates that increased only slightly with steeper pH gradients (Fig. 3*B*). With the double-mutant FocA F75A/F202A, an increase in buffer acidity led to inhibition of transport; formate/formic acid uptake was even fully blocked at external pH values below 6.3 (Fig. 3*B*). Thus, removal of the periplasmic constriction, which is oriented toward the acidic pH compartment in this experiment, results in a loss of substrate anion/H^+ cotransport. It appears possible that without the barrier, a proton may access the central histidine region. The data are therefore supportive of a transport model that is based on an unprotonated histidine and direct substrate anion protonation in the vestibule. Mutational widening of the constrictions might further render the vestibules less lipophilic because of a higher population of water molecules. A resulting smaller shift of the substrate pK_a would decrease protonation and transport efficiencies as well.

Kinetic and energetic transport parameters support the vestibular substrate protonation hypothesis

A putative electrostatic interaction of a formate anion with a protonated central histidine would be characterized by a large

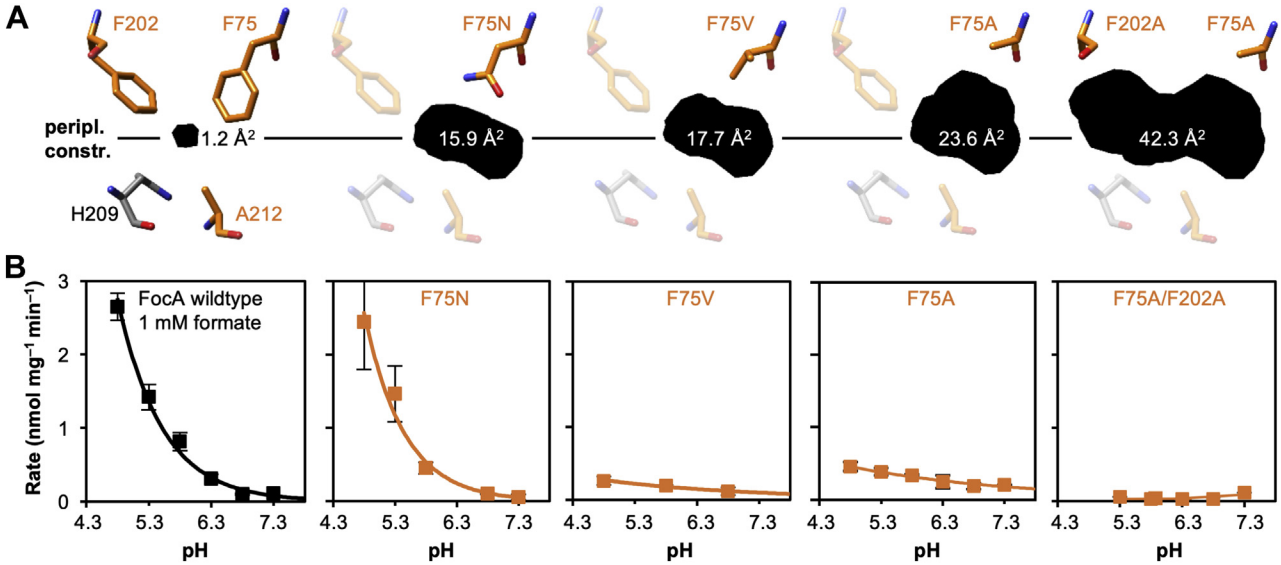

Figure 3. pH dependence of formate/formic acid transport by FocA wildtype and mutants with a widened periplasmic constriction site. *A*, models based on FocA crystal data (Protein Data Bank ID: 3KCU, chain A) showing the aperture areas in the plane through the periplasmic constriction site defined by the α-carbons of Phe75, Phe202, and Ala212. *B*, shown are the rates of formate transport at 1 mM inward substrate gradient and varying buffer pH into expressing yeast cells (W303IA Δjen1 Δady2). Error bars indicate SEM from three individual experiments each with triplicate data points. FocA, FNT-type formate transporter from *Escherichia coli*.

binding affinity (19), whereas transport of a neutralized substrate after protonation in the vestibule would be more channel like, that is, exhibiting very low affinity (11). Of the various FocA mutants with sufficient activity at neutral and slightly acidic pH, we chose FocA F75A for determining kinetic transport parameters because it contained the widest periplasmic constriction (Fig. 4). At pH 6.8, the transport rates of FocA wildtype and FocA F75A increased over the testable substrate concentration range up to 200 mM without reaching a plateau (Fig. 4*A*). From extrapolation, we estimated K_M values around 100 mM (no significant difference according to Student's *t* test) (Fig. 4*C*). Despite considerable error margins in particular for FocA F75A because of low activity and affinity values, the data clearly show the known atypical channel-like behavior because a transporter with a dedicated substrate binding site would exhibit a K_M value in the micromolar or single-digit millimolar range (20). Furthermore, FocA wildtype and FocA F75A did not significantly differ in the extrapolated v_{max} values at neutral pH (Fig. 4*E*). Switching to slightly acidic conditions of pH 5.8 led to an increased apparent affinity with equal K_M values around 16 mM for FocA wildtype and FocA F75A (Fig. 4, *B* and *D*), an effect that was also observed before (5). Besides higher availability of protons, the pH effect might also be related to the tenfold higher concentration of protonated substrate in the buffer. However, we found a clear difference between wildtype FocA and the F75A mutant in the achievable transport velocities. Transport of FocA wildtype was independent from the external pH, whereas the v_{max} of FocA F75A was decreased by a factor of 5 at pH 5.8 (Fig. 4*F*). This hints at protonation of a protein site that is not accessible in wildtype FocA with the central histidine being a plausible candidate. The observed transport block of the wider FocA F75A/F202A can be explained by a more complete histidine protonation. Intact constriction sites in FNT proteins would therefore be required to shield the central histidine from protonation.

Mutational widening of the FocA periplasmic constriction greatly increased the Arrhenius activation energy for formate/formic acid transport (Fig. 5). Wildtype FocA yielded the previously reported very low activation energy around 1 kcal mol^{-1} indicating channel-like substrate translocation (11) (Fig. 5, *A* and *D*). The activation energies of FocA F75V and FocA F75A were 13 and 17 kcal mol^{-1}, respectively (Fig. 5, *B–D*). The observed higher energetic barriers again hint a (partially) protonated central histidine enforcing the interaction with the substrate (19).

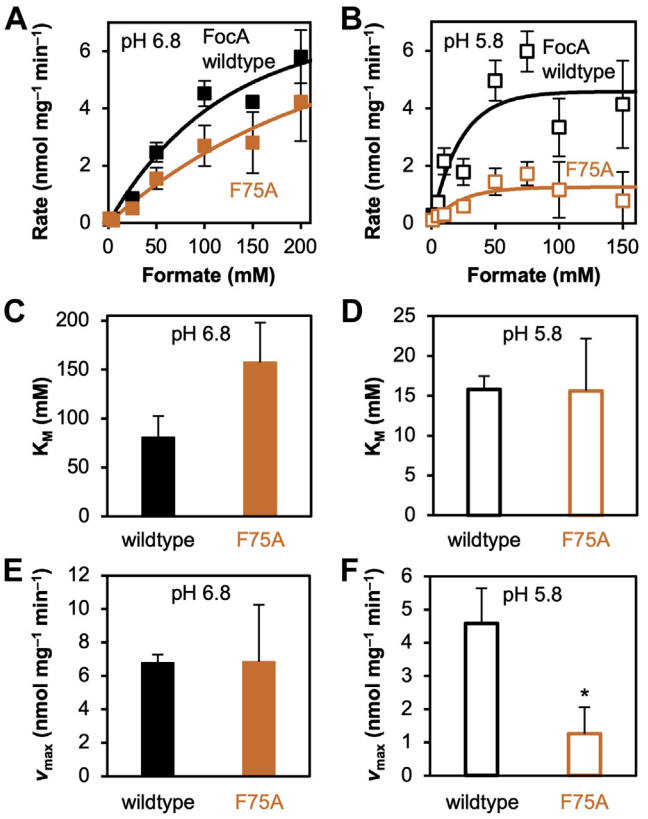

Figure 4. Kinetic parameters of formate/formic acid transport by FocA and FocA F75A at neutral and acidic pH conditions. *A* and *B*, transport dependence from the substrate concentration at pH 6.8 (*A*) and 5.8 (*B*) using yeast cells (W303IA Δjen1 Δady2). *C* and *D*, apparent Michaelis–Menten constants, K_M, obtained at pH 6.8 (*C*) and 5.8 (*D*) from the above curves. *E* and *F*, maximum velocity of transport at pH 6.8 (*E*) and 5.8 (*F*) derived from the above curves. Errors represent SEM from three independent experiments, each with triplicate data points. Only the difference in v_{max} at pH 5.8 observed between FocA wildtype and the F75A mutant (*F*) was significant ($p < 0.05$; unpaired two-tailed Student's *t* test). FocA, FNT-type formate transporter from *Escherichia coli*.

Elimination of the FocA constriction sites enables water permeability and proton flux

If a water chain connects the central histidine with the aqueous bulk in the FocA constriction mutants, water

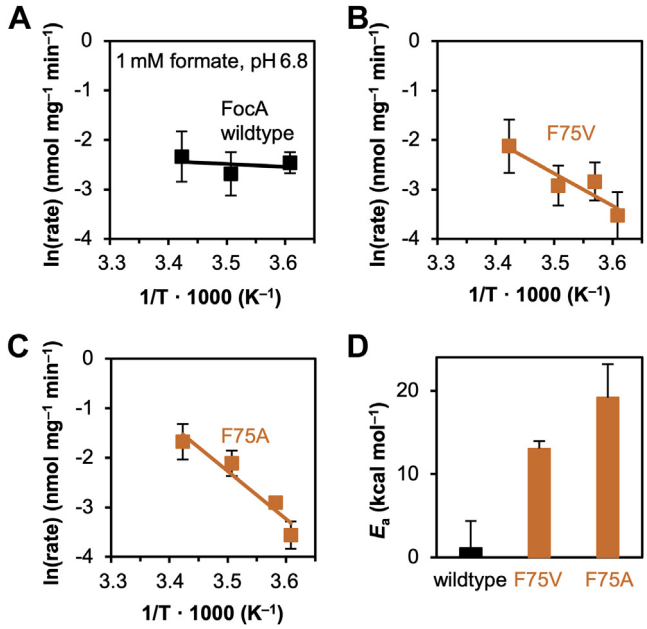

Figure 5. Temperature dependence of formate/formic acid transport. By FocA wildtype (*A*) and two mutants with single-point mutations in the periplasmic constriction (*B* and *C*) using yeast cells (W303IA Δjen1 Δady2). *D*, Arrhenius activation energies were derived from the slopes of the graphs. Error bars denote SEM from three independent experiments, each with triplicate data points. FocA, FNT-type formate transporter from *Escherichia coli*.

molecules may well pass the transduction path altogether, that is, the mutant FocA proteins could exhibit AQP-like water channel properties. We assayed osmotic water permeability of the FocA constriction mutants in a yeast strain (BY4742 Δfps1) (22) that lacks endogenous AQPs using stopped-flow light scattering for monitoring rapid cell volume changes (Fig. 6). TbAQP2 from *Trypanosoma brucei* with water and neutral solute permeability (23, 24) served as a reference (Fig. 6, *A* and *F*). As reported earlier (9), we found wildtype FocA to be impermeable to water (Fig. 6, *B* and *F*). The mutant with a widened periplasmic constriction, FocA F75A, already showed some water permeability (Fig. 6, *C* and *F*). This indicates that the cytoplasmic constriction is naturally leaky for water molecules probably because of a high flexibility of the leucine side chains. The corresponding mutation in the cytoplasmic constriction site, FocA L89A, however, maintained selectivity against water (Fig. 6, *D* and *F*) suggesting that the aromatic phenylalanine side chains of the periplasmic constriction are less pliable. The FocA F75A/F202A–L79A/L89A mutant with both constrictions widely opened enabled water permeability even higher than TbAQP2 (Fig. 6, *E* and *F*). It should be considered that permeability of neutral water is independent from a charge at the protonated central histidine, and that this mutant appeared nonfunctional before with respect to formate/formic acid transport (Fig. 2*D*).

We then asked whether a possibly continuous water chain in the transduction path of mutant FocA proteins could act as a proton wire. A proton is translocated along a proton wire by concerted alterations of the bonding character of hydrogen bonds and covalent bonds, termed the Grotthuss mechanism (25). This way, the leaving proton from the water chain is different from the one that entered the chain. To test for proton conductance, we loaded the yeast cells with pH-sensitive 6-carboxyfluorescein (6-FAM) and switched the external buffer pH to 5.2 (26). Indeed, FocA F75A/F202A–L79A/L89A with two widened constriction sites exhibited proton flux at the same time scale as water permeation, whereas FocA wildtype was at the background level (Fig. 6*G*).

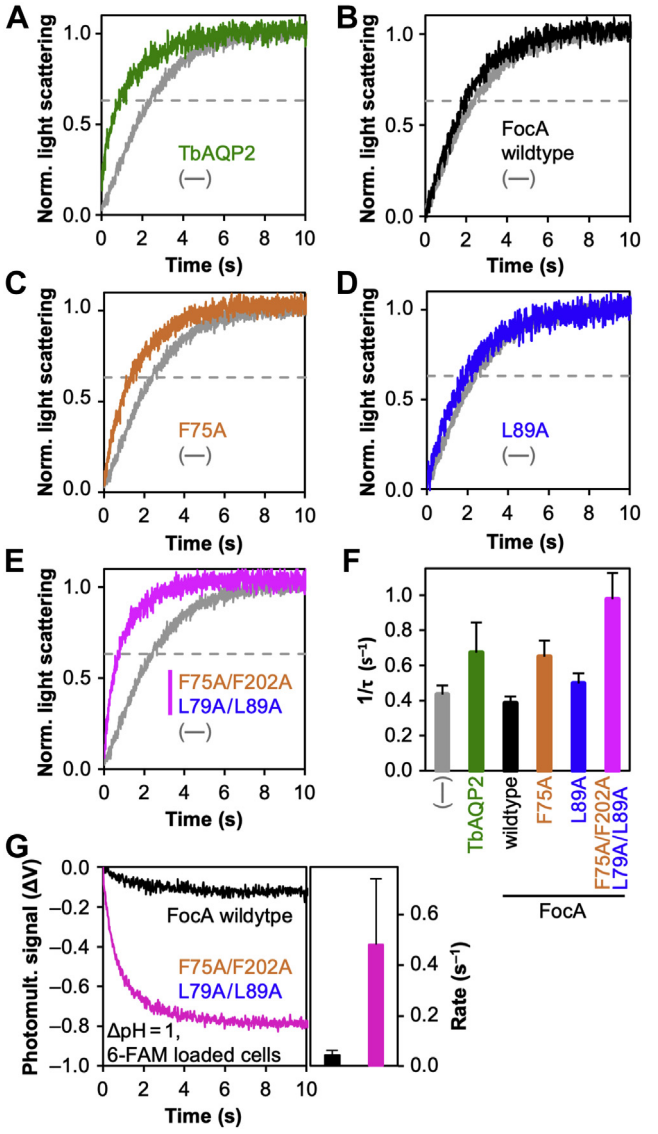

Figure 6. Water permeability and proton conductance of FocA wildtype and constriction mutants in yeast protoplasts without endogenous AQPs (BY4742 Δfps1). *A*, the *Trypanosoma brucei* AQP2 (*green*) served as a water-permeable control for the stopped-flow light scattering assay detecting cell shrinkage after osmotic challenge (300 mM sucrose gradient). Background protoplast shrinkage (–) is shown in *gray*. *B–E*, water permeability of FocA wildtype and constriction mutants compared with background. *F*, relative water permeability rates are given as the reciprocal of τ, which can be read at 63.2% completion of the process (*dotted lines*). *G*, proton influx elicited by an inward gradient of 1 pH unit (pH_{ext} 5.2 and pH_{int} 6.2) *via* FocA wildtype (*black*) or FocA F75A/F202A–L79A/L89A (*magenta*). Cytosolic pH shifts were detected by changes in the fluorescence intensity of carboxyfluorescein (6-FAM; λ_{ex} 495 nm and λ_{em} > 500 nm). Rates of proton flux were derived from single-exponential fittings of the curves after background subtraction. Error bars denote SEM from three independent experiments (two for proton flux) each with 5 to 9 recorded traces. AQP, aquaporin; FocA, FNT-type formate transporter from *Escherichia coli*.

The FocA constrictions select against permanently neutral solutes

We noticed throughout the previous experiments that yeast cells expressing FocA F75A/F202A–L79A/L89A were strongly retarded in growth (doubling time of 5.4 h) compared with cells producing the remaining constructs of this study (doubling times of 3.6–4.1 h). The size and morphology of these cells was not altered, though. Slower growth rates may be because of the observed proton leak and increased energy consumption by pH-correcting proton pumping action (27). Decreased growth rates could also be caused by newly enabled permeability properties of the mutated FocA leading to a loss of needed metabolites. In a final experiment, we tested the FocA constructs for methylamine permeability, that is, a small neutral compound that is toxic to yeast cells (Fig. 7) (28). The respective phenotypic growth rescue assay is based on the uptake the protonated and positively charged methylammonium form, $H_3C–NH_3^+$, from an acidic external buffer *via* endogenous yeast ammonium transporters, MEP1–3 (29). The more neutral cytoplasmic pH conditions shift the protonation equilibrium toward deprotonated neutral methylamine, $H_3C–NH_2$, which will be released from the cell if a

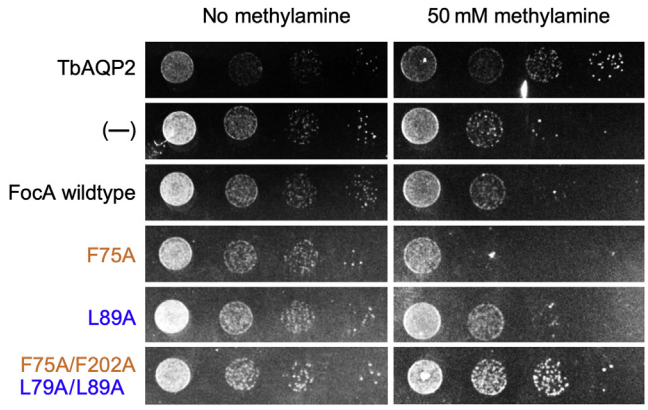

Figure 7. Phenotypic growth assay indicating permeability of FocA wildtype and constriction mutants for neutral methylamine. TbAQP2 (positive control), FocA wildtype, and constriction mutants were expressed in yeast (BY4741) without endogenous AQPs (Δfps1) and glycerol transporters (Δstl1); (––) indicates cells without endogenous AQPs and glycerol transporters. The cells were spotted in tenfold serial dilutions on selective agar media at pH 5.5 without (growth control; *left panel*) or with 50 mM methylamine/methylammonium (*right panel*). Protonated methylammonium is transported into the yeast cytosol by endogenous ammonium transporters. The less acidic cytosolic pH shifts methylammonium toward deprotonation, and the presence of a methylamine-permeable transmembrane protein enables release of the yeast-toxic compound and cell growth. AQP, aquaporin; FocA, FNT-type formate transporter from *Escherichia coli*.

channel with the respective permeability, for example, a solute-permeable AQP, is present (28). Accordingly, in this assay, growth indicates export of neutral methylamine. We spotted yeast suspensions in tenfold serial dilutions onto agar plates at pH 5.5 with 50 mM methylamine/methylammonium (Fig. 7). TbAQP2 with known methylamine permeability (30) enabled growth at the highest dilution of the yeast suspension. Nonexpressing yeast cells indicate the background of the assay. Of the FocA mutants, only F75A/F202A–L79A/L89A, in which both constriction sites were opened up, grew on the selective agar to similar levels as TbAQP2 showing methylamine permeability. As for water, passage of the neutral substrate methylamine is unhampered by a protonated central histidine.

Taken together, our experiments show that the FocA constriction sites act as barriers mainly against protons. Elimination of the constrictions enables water and neutral solute permeability but ceases formate/H^+ transport probably by a strong interaction of the substrate anion with the protonated central histidine.

Discussion

Our data provide experimental insight into the functional role of the FNT constriction sites and the central histidine. Initially, the FocA constriction sites, particularly the one on the periplasmic side, were seen as substrate selectivity filters in analogy to the AQP aromatic arginine selectivity filter (25), which is positioned in a similar location within the protein (9). Later studies described a transport rate–determining role of the FocA constriction sites after observing higher uptake capacities when widening mutations were introduced (14, 21). However, in the *Plasmodium* FNT, replacement of a phenylalanine of the extracellular constriction by alanine decreased the rate transport by half (31). In this study, we confirmed the notion of a higher uptake capacity with the FocA F75A single mutation. Yet, further widening of the constriction sites by the introduction of double alanine mutations led to a loss of formate/formic acid transport functionality. This shows that the diameters of the constriction sites and the side-chain flexibility of the forming amino acids are balanced to allow for optimal substrate passage. A too narrow constriction will exclude larger substrates by size. But why would a wider constriction impede transport?

The altered pH dependence of the mutants of this study links the constriction sites to protonation events. While the formate/formic acid transport rate of wildtype FNTs increases with the availability of protons in the buffer (5, 11), this behavior was lost or transport even fully ceased with the FocA constriction mutants except for FocA F75N with the smallest change in the constriction diameter. Although hydrophobicity was maintained with the introduction of valine or alanine residues, the replacement of bulky phenylalanine or leucine residues gives room for additional water molecules to enter the transport pathway alongside the substrate. This is seen by the gain of water permeability of certain FocA mutants. As a result, in a dielectric slide mechanism scenario (16), the substrate pK_a will be less disturbed than in a truly hydrophobic environment decreasing the protonation efficiency and transport rates. The gain of a proton conductance with enabled water permeability in mutant FocA indicates that, different from the AQPs that have sophisticated mechanisms to exclude protons from a water chain (32, 33), the FNT constriction sites act as barriers blocking both, water and protons. Therefore, in an FNT transport model that requires a protonated central histidine (17), transport activity should be increased with widened constrictions. However, this was not observed in our experiments.

Besides protons, the constriction sites also seem to select against small neutral molecules as exemplified by the phenotypic methylamine assay. Yet, the dielectric slide mechanism also assumes passage of the neutral weak acid substrate across the constriction sites. Previous studies on other weak acid transport proteins showed that electrostatic attraction of the substrate anion by positive amino acid residues facilitates higher transport rates by an increased local substrate concentration and protonation efficiency than in the aqueous bulk (26, 34). Accordingly, only weak acid substrates can pass the double check points of the FNT transport path that test for two molecule properties, namely a negative charge (*via* attraction) and a proton-acceptor site (for neutralization). The presence of two constrictions in the FNTs further indicates that their main function is not in substrate size selection, for which a single filter region would suffice (aromatic arginine region in AQPs, Φ/K in FNTs) (25, 35) but in proton exclusion from the central histidine region.

The FocA protomer holds a total of six histidine residues. Five of which are located in positions that are exposed to the solvent resulting in predicted pK_a values (36) of around 6, that

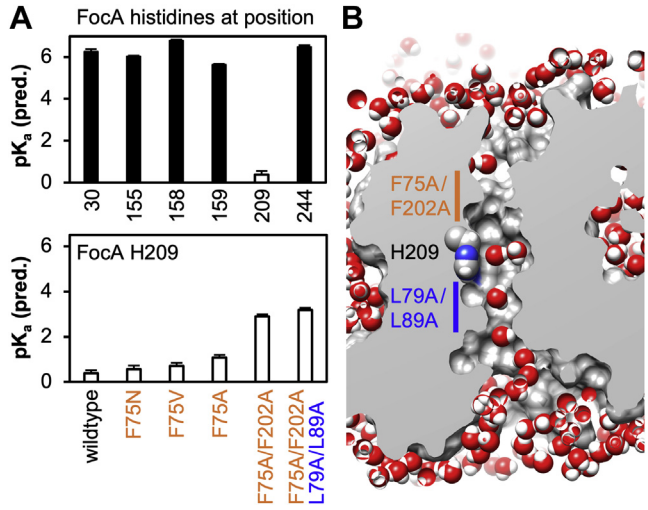

Figure 8. Predictions of histidine pK_a values in FocA wildtype and constriction mutants and solvation by water of the FocA F75A/F202A–L79A/L89A mutant. *A*, six histidine residues are present in the FocA protomer at positions 30, 155, 158, 159, 209, and 244 (Protein Data Bank ID: 3KCU). The DEPTH algorithm was used to predict respective pK_a values (*top panel*). Effects of constriction-widening mutations on the pK_a of the central His209 are shown in the *lower panel*. *B*, solvation simulations by water of the FocA F75A/F202A–L79A/L89A mutant indicates connecting water chains from the bulk to the central histidine (here from the cytoplasmic side) that may act at proton wires. FocA, FNT-type formate transporter from *Escherichia coli*.

is, equaling that of a freely dissolved histidine (Fig. 8*A*, *upper panel*). The pK_a of the central histidine at position 209, however, was calculated to 0.4. With an acid strength more than five orders of magnitude higher than in solution, the central histidine must be expected to be deprotonated essentially at all times. This situation is permanently given in FNT isoforms that naturally hold a nonprotonatable residue in this position such as asparagine in the *E. histolytica* FNT (15). Predictions of solvation by water (37) of FocA F75A/F202A–L79A/L89 showed single-file passage at the enlarged constriction sites with the cytoplasmic site being slightly wider than the periplasmic one and enough space for two water molecules in the central histidine region (Fig. 8*B*). Accordingly, the predicted pK_a of His209 was raised to 3.2 (Fig. 8*A*, *lower panel*) enabling considerable protonation.

Would it be possible to convert an AQP into a monocarboxylate/H^+ transporting FNT? In fact, there are AQP isoforms, for example, human AQP9 (34), which exhibits some lactate/H^+ transport. A key difference in the protein structures is the shallowness of the vestibules in the AQPs compared with the FNTs (11, 16, 26). The FNT-typical dielectric slide mechanism requires that the weak acid substrate enters a lipophilic environment that results in a shift of the acidity. Certain AQPs carry clusters of positively charged residues (eight arginines in the AQP9 tetramer) at the protein surface close to the pore entry that are thought to locally concentrate lactate anions facilitating protonation and eventually passage (38). However, because of the solvent exposure, this process is much less efficient than that of an FNT, that is, a dedicated monocarboxylate/H^+ transporter with a positive lysine situated deep inside a lipophilic vestibule (26).

In conclusion, we found that intact FNT constriction sites are essential for weak acid/H^+ transport. We provide evidence that the key task of the constriction sites is to protect the highly conserved central histidine from protonation by breaking water chains and proton wires. The neutral central histidine apparently has mainly structural functions rather than a role in proton transfer similar to two conserved and unprotonated histidine residues in the transport pathway of ammonium transporters (39).

Experimental procedures

Plasmids, mutations, yeast transformation, and culture

The *E. coli* FocA construct encoding an additional N-terminal hemagglutinin tag and a C-terminal His_{10} tag in the yeast expression vector pDR196 as well as *T. brucei* TbAQP2 in pRS426Met25 was previously described (11, 23). Point mutations were introduced using the QuickChange protocol (Stratagene) and primers with respective nucleotide exchanges in the forward primer (Thermo Fisher Scientific). Mutation primers used were: F75A, GTT GGC GGC ATT TGC GCA TCT CTG GGG; F75V, GGC GGC ATT TGC GTC TCT CTG GGG CTG ATT; F75N, GGC GGC ATT TGC AAC TCT CTG GGG CTG ATT; F202A, CCG GTC GCG ATG GCT GTT GCC AGC GGT TTT; L79A, TCT CTG GGG GCG ATT CTT TGT GTT GTC T; L89A, TGC GGA GCC GAT GCA TTT ACT TCC ACC GTG. All constructs were sequenced for verification (IKMB). *S. cerevisiae* yeast was transformed using the lithium actetate/single-stranded carrier DNA/polyethylene glycol procedure (40) and grown at 29 °C on selective dropout media without uracil.

Preparation of yeast microsomal proteins and Western blotting

About 50 ml yeast cultures were grown to an absorbance of 1.0 ± 0.2 at 600 nm, harvested (4000*g*, 5 min), washed with 20 ml of ice-cold water, and resuspended in 500 µl buffer (5 mM EDTA, 25 mM Tris, and pH 7.5). The cells were disrupted by vortexing with 500 µg acid-washed glass beads (450–600 µm; Sigma–Aldrich) for 30 s and cooling on ice for 1 min with 12 repetitions. The supernatant was collected (4000*g*, 5 min), and the procedure was repeated with the remaining pellet. The microsomal fraction was obtained by removal of high-density components (10,000*g*, 5 min, 4 °C) and ultracentrifugation (100,000*g*, 45 min, 4 °C). The membrane pellets were resuspended in 0.1 ml of 50 mM NaCl, 100 mM sodium phosphate, pH 8.0. About 7.5 µg of total protein (Bradford Protein Assay; Bio-Rad) were separated by SDS-PAGE and blotted (semidry; Bio-Rad) on Polyvinylidene fluoride membranes (Hybond P 0.45; GE Healthcare). A monoclonal mouse antihemagglutinin antibody (catalog number: 34660; Qiagen) and a horseradish peroxidase–conjugated secondary goat–antimouse antibody (catalog number: 115-035-174; Jackson ImmunoResearch) were used for detection with the Clarity ECL system (Bio-Rad). Signals were monitored using a Chemostar Touch ECL & Fluorescence Imager (Intas Science Imaging Instruments).

Formate/formic acid uptake assay

The uptake of ^{14}C-radiolabeled formate/formic acid was assayed as described before (5, 20). Briefly, W303IA Δjen1 Δady2 yeast cells kindly provided by M. Casal (41) expressing FocA wildtype or mutants were harvested (4000*g*, 5 min) at an absorbance of 1.0 ± 0.1 at 600 nm, washed with ice-cold water, and resuspended to an absorbance of 50 ± 5 at 600 nm in buffer (50 mM Hepes/Tris for pH 7.3–6.3; 50 mM Mes/Tris for pH 5.8–5.3; 50 mM citric acid/Tris for pH < 5.3). To initiate uptake, samples of 80 µl, corresponding to 5.6 mg dry weight yeast, were rapidly mixed at 19 °C with 20 µl formate solution spiked with ^{14}C-formate (0.04–0.24 µCi depending on the formate gradient; Hartmann Analytics). Uptake was stopped by adding of 1 ml ice-cold water and rapid filtration of the sample *via* a GF/C glass microfiber filter (0.45 µm; GE Healthcare). The filters were washed with 7 ml of ice-cold water to remove excess substrate and dissolved in 3 ml of scintillation cocktail (Quicksafe A, Zinsser Analytic) for scintillation counting (Packard TriCarb 2900TR; PerkinElmer). Each data point is a mean of at least three independent experiments with three replicates each; error bars denote SEM. For time curves, the replicates were carried out in 96-well filter plates (Multiscreen HTS 96 HV Filter Plate, opaque, 0.45 µm and vacuum manifold; Merck). Here, cells were washed with 600 µl of ice-cold water. Then, 200 µl of scintillation cocktail (MicroScint-20; PerkinElmer) were added for counting (MicroBeta Trilux Counter; PerkinElmer). For data analysis, outliers were determined according to Henning (mean ± 3 s), and normality of the samples was verified using the David–Hartley–Pearson test (p = 0.95). Variance homogeneity was checked by F test (p = 0.95), and depending on the outcome, significance was tested using Student's t test (unpaired and two-tailed) or Welch's test (p = 0.95).

Protein models, pK_a predictions, and solvation

Protein structure models of *E. coli* FocA (PDB ID: 3KCU) (9) were generated and analyzed using PyMol (The PyMOL Molecular Graphics System, version 1.7.4.1; Schrödinger, LLC) and Chimera (37). The open diameter in the plane of the periplasmic constriction site defined by the α-carbons of Phe75, Phe202, and Ala212 was determined from images of the protein surface display using ImageJ (National Institutes of Health) (42). Predictions of histidine pK_a values were done using the Residue Depth algorithm using the SPC216 water model and setting of the water cluster size to at least two neighboring water molecules (43). Solvation of the FocA F75A/F202A–L79A/L89A transport path was done with chimera using the TIP3PBOX solvation model and a 5 Å water shell (37).

Yeast protoplast preparation, water permeability, and proton conductance assays

About 50 ml of BY4742 Δfps1 yeast cultures (Euroscarf), lacking the endogenous AQP Fps1 (22), were transformed, grown, and harvested by centrifugation (4000*g*, 4 °C), washed once, and resuspended in 2 ml buffer (2-mercaptoethanol, 50 mM Mops, and 0.2% pH 7.2). Cells were brought to 30 °C for 15 min on an orbital shaker at 140 rpm. About 4 ml of 0.2% 2-mercaptoethanol, 50 mM Mops, and pH 7.2, supplemented with 1.2 M sucrose, 100 mg albumin fraction V (Roth), and 120 U zymolyase-20T (Roth). After 1 h of protoplastation, cells were collected (2000*g*, 4 °C), washed, and adjusted to an absorbance of 2 at 600 nm with 10 mM Mops, 50 mM NaCl, 5 mM $CaCl_2$, 1.2 M sucrose, and pH 7.2. For testing water permeability, yeast protoplast suspensions were rapidly mixed in a stopped-flow apparatus (SFM-2000; BioLogic) with an equal volume of the same buffer, yet containing 1.8 M sucrose establishing an outward osmotic gradient of 300 mOsm kg^{-1}. Protoplast shrinkage was monitored for 12 s as an increase in the intensity of 90° light scattering at 524 nm. For proton conductance measurements, yeast cells were incubated at 29 °C with 100 µM 6-FAM diacetate *N*-succinimidyl ester (Sigma–Aldrich) in 50 mM Mops, pH 7.2, for 24 h, and washed five times 50 mM Mops, pH 7.2, prior to protoplastation. To establish an inward transmembrane pH gradient of 1 unit, loaded yeast cells were mixed in a stopped-flow device with an equal volume of 50 mM NaCl, 5 mM $CaCl_2$, 1.2 M sucrose, 10 mM Mops, and pH 5.2. The resulting pH was 6.2 as checked using a pH electrode (Blue Line 12pH; SI-Analytics). Fluorescence was excited at 495 nm and monitored for 12 s using a filter with <500 nm cutoff. Data were averaged from three independent experiments (two for proton conductance) with 5 to 9 traces each and normalized. Relative water permeability rates were expressed as reciprocals of the τ values; error bars denote SEM.

Phenotypic yeast assays for methylamine permeability

BY4741 Δfps1 Δstl1 yeast (kindly provided by H. Sychrova), lacking the endogenous AQP Fps1 (22) and the glycerol transporter Stl1 (44), was transformed, grown, and harvested (30 s, 21,000*g*). The cells were washed and resuspended to an absorbance of 1 ± 0.1 in water. About 5 µl of serial tenfold suspension dilutions were spotted on selective dropout agar media (0.17% yeast nitrogen base, 2% glucose, 0.1% proline, 0.002% lysine, 0.002% histidine, 0.01% leucine, 20 mM Mes, pH 5.5, plus 2% Oxoid agar) with and without 50 mM methylamine. Plates were kept at 29 °C for up to 11 days.

Data availability

All data are contained within the article.

Acknowledgments—We thank A. Fuchs for excellent technical assistance and N.H. Epalle for help with the 6-FAM assay. We thank the Institute of Clinical Molecular Biology in Kiel for providing Sanger sequencing as supported in part by the DFG Clusters of Excellence "Precision Medicine in Chronic Inflammation" and "ROOTS." We thank T. Naujoks, Dr D. Langfeldt, and Dr B. Löscher for technical support.

Author contributions—E. B. conceptualization; J. D. R. S. and E. B. formal analysis; J. D. R. S. investigation; J. D. R. S. and E. B. writing–original draft; J. D. R. S. and E. B. writing–review & editing; E. B. supervision.

Funding and additional information—This work was funded by the Deutsche Forschungsgemeinschaft (Be2253/8-2) and the European Union's Horizon 2020 research and innovation program under the Marie Skłodowska-Curie grant agreement no. 860592 (PROTON).

Conflict of interest—The authors declare that they have no conflicts of interest with the contents of this article.

Abbreviations—The abbreviations used are: 6-FAM, 6-carboxyfluorescein; AQP, aquaporin; FNT, formate–nitrite transporter; FocA, FNT-type formate transporter from *Escherichia coli*; PDB, Protein Data Bank.

References

1. Mukherjee, M., Vajpai, M., and Sankararamakrishnan, R. (2017) Anion-selective formate/nitrite transporters: Taxonomic distribution, phylogenetic analysis and subfamily-specific conservation pattern in prokaryotes. *BMC Genomics* **18**, 560
2. Sawers, R. G. (2005) Formate and its role in hydrogen production in *Escherichia coli*. *Biochem. Soc. Trans.* **33**, 42–46
3. Lü, W., Du, J., Schwarzer, N. J., Gerbig-Smentek, E., Einsle, O., and Andrade, S. L. A. (2012) The formate channel FocA exports the products of mixed-acid fermentation. *Proc. Natl. Acad. Sci. U. S. A.* **109**, 13254–13259
4. Jia, W., Tovell, N., Clegg, S., Trimmer, M., and Cole, J. (2009) A single channel for nitrate uptake, nitrite export and nitrite uptake by *Escherichia coli* NarU and a role for NirC in nitrite export and uptake. *Biochem. J.* **417**, 297–304
5. Wu, B., Rambow, J., Bock, S., Holm-Bertelsen, J., Wiechert, M., Blancke Soares, A., Spielmann, T., and Beitz, E. (2015) Identity of a *Plasmodium* lactate/H(+) symporter structurally unrelated to human transporters. *Nat. Commun.* **6**, 6284
6. Golldack, A., Henke, B., Bergmann, B., Wiechert, M., Erler, H., Blancke Soares, A., Spielmann, T., and Beitz, E. (2017) Substrate-analogous inhibitors exert antimalarial action by targeting the *Plasmodium lactate* transporter PfFNT at nanomolar scale. *PLoS Pathog.* **13**, e1006172
7. Walloch, P., Henke, B., Häuer, S., Bergmann, B., Spielmann, T., and Beitz, E. (2020) Introduction of scaffold nitrogen atoms renders inhibitors of the malarial l-lactate transporter, PfFNT, effective against the Gly107Ser resistance mutation. *J. Med. Chem.* **63**, 9731–9741
8. Walloch, P., Hansen, C., Priegann, T., Schade, D., and Beitz, E. (2021) Pentafluoro-3-hydroxy-pent-2-en-1-ones potently inhibit FNT-type lactate transporters from all five human-pathogenic *Plasmodium* species. *ChemMedChem* **16**, 1283–1289
9. Wang, Y., Huang, Y., Wang, J., Cheng, C., Huang, W., Lu, P., Xu, Y.-N., Wang, P., Yan, N., and Shi, Y. (2009) Structure of the formate transporter FocA reveals a pentameric aquaporin-like channel. *Nature* **462**, 467–472
10. Murata, K., Mitsuoka, K., Hirai, T., Walz, T., Agre, P., Heymann, J. B., Engel, A., and Fujiyoshi, Y. (2000) Structural determinants of water permeation through aquaporin-1. *Nature* **407**, 599–605
11. Wiechert, M., and Beitz, E. (2017) Mechanism of formate-nitrite transporters by dielectric shift of substrate acidity. *EMBO J.* **36**, 949–958
12. Lü, W., Du, J., Wacker, T., Gerbig-Smentek, E., Andrade, S. L. A., and Einsle, O. (2011) pH-dependent gating in a FocA formate channel. *Science* **332**, 352–354
13. Lü, W., Schwarzer, N. J., Du, J., Gerbig-Smentek, E., Andrade, S. L. A., and Einsle, O. (2012) Structural and functional characterization of the nitrite channel NirC from Salmonella typhimurium. *Proc. Natl. Acad. Sci. U. S. A.* **109**, 18395–18400
14. Hunger, D., Doberenz, C., and Sawers, R. G. (2014) Identification of key residues in the formate channel FocA that control import and export of formate. *Biol. Chem.* **395**, 813–825
15. Helmstetter, F., Arnold, P., Höger, B., Petersen, L. M., and Beitz, E. (2019) Formate-nitrite transporters carrying nonprotonatable amide amino acids instead of a central histidine maintain pH-dependent transport. *J. Biol. Chem.* **294**, 623–631
16. Wiechert, M., and Beitz, E. (2017) Formate-nitrite transporters: Monoacids ride the dielectric slide. *Channels* **11**, 365–367
17. Lü, W., Du, J., Schwarzer, N. J., Wacker, T., Andrade, S. L. A., and Einsle, O. (2013) The formate/nitrite transporter family of anion channels. *Biol. Chem.* **394**, 715–727
18. Lv, X., Liu, H., Ke, M., and Gong, H. (2013) Exploring the pH-dependent substrate transport mechanism of FocA using molecular dynamics simulation. *Biophys. J.* **105**, 2714–2723
19. Atkovska, K., and Hub, J. S. (2017) Energetics and mechanism of anion permeation across formate-nitrite transporters. *Sci. Rep.* **7**, 12027
20. Köpnick, A.-L., Jansen, A., Geistlinger, K., Epalle, N. H., and Beitz, E. (2021) Basigin drives intracellular accumulation of L-lactate by harvesting protons and substrate anions. *PLoS One* **16**, e0249110
21. Czyzewski, B. K., and Wang, D.-N. (2012) Identification and characterization of a bacterial hydrosulphide ion channel. *Nature* **483**, 494–497
22. Luyten, K., Albertyn, J., Skibbe, W. F., Prior, B. A., Ramos, J., Thevelein, J. M., and Hohmann, S. (1995) Fps1, a yeast member of the MIP family of channel proteins, is a facilitator for glycerol uptake and efflux and is inactive under osmotic stress. *EMBO J.* **14**, 1360–1371
23. Uzcategui, N. L., Szallies, A., Pavlovic-Djuranovic, S., Palmada, M., Figarella, K., Boehmer, C., Lang, F., Beitz, E., and Duszenko, M. (2004) Cloning, heterologous expression, and characterization of three aquaglyceroporins from *Trypanosoma brucei*. *J. Biol. Chem.* **279**, 42669–42676
24. Song, J., Baker, N., Rothert, M., Henke, B., Jeacock, L., Horn, D., and Beitz, E. (2016) Pentamidine is not a permeant but a nanomolar inhibitor of the *Trypanosoma brucei* aquaglyceroporin-2. *PLoS Pathog.* **12**, e1005436
25. Beitz, E., Wu, B., Holm, L. M., Schultz, J. E., and Zeuthen, T. (2006) Point mutations in the aromatic/arginine region in aquaporin 1 allow passage of urea, glycerol, ammonia, and protons. *Proc. Natl. Acad. Sci. U. S. A.* **103**, 269–274
26. Bader, A., and Beitz, E. (2020) Transmembrane facilitation of lactate/H^+ instead of lactic acid is not a question of semantics but of cell viability. *Membranes* **10**, 236
27. Serrano, R., Kielland-Brandt, M. C., and Fink, G. R. (1986) Yeast plasma membrane ATPase is essential for growth and has homology with (Na^+ + K^+), K^+- and Ca^{2+}-ATPases. *Nature* **319**, 689–693
28. Wu, B., Altmann, K., Barzel, I., Krehan, S., and Beitz, E. (2008) A yeast-based phenotypic screen for aquaporin inhibitors. *Eur. J. Physiol.* **456**, 717–720
29. Marini, A. M., Soussi-Boudekou, S., Vissers, S., and Andre, B. (1997) A family of ammonium transporters in *Saccharomyces cerevisiae*. *Mol. Cell. Biol.* **17**, 4282–4293
30. Zeuthen, T., Wu, B., Pavlovic-Djuranovic, S., Holm, L. M., Uzcategui, N. L., Duszenko, M., Kun, J. F. J., Schultz, J. E., and Beitz, E. (2006) Ammonia permeability of the aquaglyceroporins from *Plasmodium falciparum*, *Toxoplasma gondii* and *Trypanosoma brucei*. *Mol. Microbiol.* **61**, 1598–1608
31. Lyu, M., Su, C.-C., Kazura, J. W., and Yu, E. W. (2021) Structural basis of transport and inhibition of the *Plasmodium falciparum* transporter PfFNT. *EMBO Rep.* **22**, e51628
32. Wu, B., Steinbronn, C., Alsterfjord, M., Zeuthen, T., and Beitz, E. (2009) Concerted action of two cation filters in the aquaporin water channel. *EMBO J.* **28**, 2188–2194
33. Eriksson, U. K., Fischer, G., Friemann, R., Enkavi, G., Tajkhorshid, E., and Neutze, R. (2013) Subangstrom resolution X-ray structure details aquaporin-water interactions. *Science* **340**, 1346–1349
34. Rothert, M., Rönfeldt, D., and Beitz, E. (2017) Electrostatic attraction of weak monoacid anions increases probability for protonation and passage through aquaporins. *J. Biol. Chem.* **292**, 9358–9364
35. Wiechert, M., Erler, H., Golldack, A., and Beitz, E. (2017) A widened substrate selectivity filter of eukaryotic formate-nitrite transporters enables high-level lactate conductance. *FEBS J.* **284**, 2663–2673
36. Chakravarty, S., and Varadarajan, R. (1999) Residue depth: A novel parameter for the analysis of protein structure and stability. *Structure* **7**, 723–732
37. Pettersen, E. F., Goddard, T. D., Huang, C. C., Couch, G. S., Greenblatt, D. M., Meng, E. C., and Ferrin, T. E. (2004) UCSF Chimera–a

visualization system for exploratory research and analysis. *J. Comput. Chem.* **25**, 1605–1612
38. Schmidt, J. D. R., Walloch, P., Höger, B., and Beitz, E. (2021) Aquaporins with lactate/lactic acid permeability at physiological pH conditions. *Biochimie* **188**, 7–11
39. Khademi, S., O'Connell, J., 3rd, Remis, J., Robles-Colmenares, Y., Miercke, L. J., and Stroud, R. M. (2004) Mechanism of ammonia transport by Amt/MEP/Rh: Structure of AmtB at 1.35 A. *Science* **305**, 1587–1594
40. Gietz, R. D., Schiestl, R. H., Willems, A. R., and Woods, R. A. (1995) Studies on the transformation of intact yeast cells by the LiAc/SS-DNA/PEG procedure. *Yeast* **11**, 355–360
41. Soares-Silva, I., Paiva, S., Diallinas, G., and Casal, M. (2007) The conserved sequence NXXS/THXS/TQDXXXT of the lactate/pyruvate:H(+) symporter subfamily defines the function of the substrate translocation pathway. *Mol. Membr. Biol.* **24**, 464–474
42. Schneider, C. A., Rasband, W. S., and Eliceiri, K. W. (2012) NIH image to ImageJ: 25 years of image analysis. *Nat. Methods* **9**, 671–675
43. Tan, K. P., Nguyen, T. B., Patel, S., Varadarajan, R., and Madhusudhan, M. S. (2013) Depth: A web server to compute depth, cavity sizes, detect potential small-molecule ligand-binding cavities and predict the pK_a of ionizable residues in proteins. *Nucleic Acids Res.* **41**, W314–421
44. Ferreira, C., van Voorst, F., Martins, A., Neves, L., Oliveira, R., Kielland-Brandt, M. C., Lucas, C., and Brandt, A. (2005) A member of the sugar transporter family, Stl1p is the glycerol/H^+ symporter in *Saccharomyces cerevisiae*. *Mol. Biol. Cell* **16**, 2068–2076